*chemengineering*

MDPI

*Article*

# In Silico Study of the Influence of Various Substrates on the Electronic Properties and Electrical Conductivity of Mono- and Bilayer Films of Armchair Single-Walled Carbon Nanotubes

**Michael M. Slepchenkov [1], Alexander A. Petrunin [1] and Olga E. Glukhova [1,2,*]**

[1] Institute of Physics, Saratov State University, Astrakhanskaya Street 83, 410012 Saratov, Russia; slepchenkovm@mail.ru (M.M.S.); sacha.petrynin@gmail.com (A.A.P.)
[2] Laboratory of Biomedical Nanotechnology, I.M. Sechenov First Moscow State Medical University, Trubetskaya Street 8-2, 119991 Moscow, Russia
* Correspondence: glukhovaoe@info.sgu.ru; Tel.: +7-8452-514562

**Abstract:** We investigate electronic and electro-physical properties of mono- and bilayer armchair single-walled carbon nanotube (SWCNT) films located on substrates of different types, including substrates in the form of crystalline silicon dioxide ($SiO_2$) films with $P4_2/mnm$ and $P3_121$ space symmetry groups. The SWCNT films interact with substrate only by van der Waals forces. The densities of electronic states (DOS) and the electron transmission functions are calculated for SWCNT films with various substrates. The electrical conductivity of SWCNT films is calculated based on the electron transmission function. It is found that the substrate plays an important role in the formation of DOS of the SWCNT films, and the surface topology determines the degree and nature of the mutual influence of the nanotube and the substrate. It is shown that the substrate affects the electronic properties of monolayer films, changing the electrical resistance value from 2% to 17%. However, the substrate has practically no effect on the electrical conductivity and resistance of the bilayer film in both directions of current transfer. In this case, the values of the resistances of the bilayer film in both directions of current transfer approach the value of ~6.4 kΩ, which is the lowest for individual SWCNT.

**Keywords:** electrical conductivity; carbon nanotubes; thin films; silicon oxide; electronic band structure; electron transmission function



**Citation:** Slepchenkov, M.M.; Petrunin, A.A.; Glukhova, O.E. In Silico Study of the Influence of Various Substrates on the Electronic Properties and Electrical Conductivity of Mono- and Bilayer Films of Armchair Single-Walled Carbon Nanotubes. *ChemEngineering* **2021**, *5*, 48. https://doi.org/10.3390/chemengineering5030048

Academic Editor: Andrew S. Paluch

Received: 1 July 2021
Accepted: 6 August 2021
Published: 9 August 2021



## 1. Introduction

One of the most relevant topics in modern science and engineering is the search for thin flexible conductive films for different applications in electronics. At present, carbon nanotubes (CNTs) are the most promising materials for creating such films [1–10]. As is known, CNT-based thin films with a thickness in the range of 1–100 nm have high electrical conductivity, transmittance, flexibility and stretchability [2]. In addition to these properties, CNT-based films are easier and cheaper in production, and therefore more competitive in comparison with other materials used to fabricate flexible and transparent electronics devices [11,12]. In particular, CNT films are superior in flexibility and extensibility to thin films based on indium tin oxide (ITO) and metal nanowires films. In addition, the metal nanowires films are inferior to CNT-based films in thermal stability, and ITO films are not suitable for mass production due to the high cost of the rare element indium [13]. CNT-based films are synthesized mainly with randomly oriented CNTs [6–10], but the technology for obtaining thin films with well-ordered parallel CNTs has been developed in recent years [14,15]. Highly conductive metallic CNT films with 40–70% optical transmittance in the visible range with a film thickness of 0.1–1 μm are already used [2]. Using long CNTs (~10 μm), Mirri et al. produced uniform films with a sheet resistance of ~100 Ω/sq at ~90% transmittance in the visible wavelength range by scalable dip-coating [6]. Today,

the process of manufacturing such films is sufficiently mastered. In addition, low-cost inkjet printing methods for the production of SWCNTs and SWCNT-based composites are already widely used at the moment [7–9,16]. The first examples of highly stretchable all-printed CNT-based electrochemical sensors and high-performance thin-film transistors were obtained [17–19]. Cai et al. designed and fabricated a transparent and super-stretchable CNT-based capacitive strain sensor that could detect strains up to 300% with high sensitivity and excellent durability even after thousands of cycles [20]. Dinh et al. demonstrated the CNT-based sensitive wearable thermal flow sensor for the noninvasive monitoring of human respiration [21]. The $Fe_2O_3$/CNTs composites have been recognized as anode materials for a new generation of lithium-ion batteries [22].

It is predicted that CNT-based electronics are a potential candidate to replace silicon complementary metal-oxide-semiconductor (CMOS) technology used for fabricating the elements of electronic circuits [19,23–26]. According to Franklin, the ideal material for high-performance CNT-based electronics is a parallel array film of SWCNTs [27]. Integrated circuits in the gigahertz range based on films of SWCNTs are already being developed [28–30]. In particular, Zhong et al. developed the SWCNT-based top-gate field-effect transistor (FETs) with a high current density of 0.55 $mA\mu m^{-1}$ and transconductance of 0.46 $mS\mu m^{-1}$ at a supply voltage of 0.8 V, and five-stage ring oscillators based on optimized FETs with an oscillation frequency of up to 5.54 GHz [28]. Xie et al. proposed 3D integrated circuits technology that promotes the operation speed of CNT-based FETs. Using this technology, researchers have created 3D five-stage ring-oscillator circuits with an oscillation frequency of up to 680 MHz and a stage delay of 0.15 ns [29].

Nevertheless, the further improving electrical conductivity of CNT films still remains a challenging unsolved problem. It is required to carry out detailed scientific research using computer simulation methods to reveal the mechanisms for controlling the transport of electrons in CNT films at the quantum level. In this paper, in silico methods are used to study the electronic properties of mono- and bilayer films of armchair SWCNTs located on a $SiO_2$ substrate. This type of substrate was chosen because silicon dioxide $SiO_2$ is widely used in the manufacture of electronic devices and, in particular, carbon nanodevices [31–34]. We considered SWCNTs of the type (m, m) for m = 4, 5, 6 and 7 with a diameter from 5 Å to 10 Å, that is, nanotubes of sub- and nanometer diameters. The choice of armchair nanotubes is due, first, to the metallic type of conductivity and, second, to the absence of chirality. Achiral nanotube allows matching the translation vector of the nanotube with the translation vector of the substrate, which is not realized for chiral nanotubes. The metallic type of conductivity of the SWCNTs is chosen to clarify the effect of the substrate on the electrical conductivity.

## 2. Computational Details

To study the electronic properties, in particular, the band structure, the SCC-DFTB (self-consistent charge density functional tight-binding) method was used [35,36]. This method has been proven in studies of the electronic properties of new composite materials, including carbon composite materials [37–39]. The total energy of the system within this approach is determined by the expression:

$$E_{tot} = \sum_{i\mu v} c_{\mu}^{i} c_{v}^{i} H_{\mu v}^{0} + \frac{1}{2} \sum_{\alpha\beta} \gamma_{\alpha\beta} \Delta q_{\alpha} \Delta q_{\beta} + E_{rep} + E_{dis}, \quad (1)$$

where $c_{\mu}^{i}$ and $c_{v}^{i}$ are the weight coefficients in the extension in atomic orbitals, $\Delta q_{\alpha}$ and $\Delta q_{\beta}$ are charge fluctuations on atoms $\alpha$ and $\beta$, accordingly, $\gamma_{\alpha\beta}$ is a function that exponentially decreases with increasing distance between atoms $\alpha$ and $\beta$, $E_{rep}$ is a term describing repulsive interaction at small distances, $E_{dis}$ is the van der Waals interaction energy between nanotubes and a substrate. The van der Waals interaction was modeled using the universal force field (UFF), which describes the interaction between various atoms [40]. The calculations were carried out in the sp-basis. We also used the Monkhorst-Pak $12 \times 12 \times 1$ scheme for the partition of the first Brillouin zone. The search for an equilibrium atomic

configuration of the film—substrate supercell was carried out by minimizing the total energy of system (1) by varying all coordinates of all atoms of the supercell. The SCC-DFTB calculations were performed using the DFTB+ software package version 20.2 [41,42].

To study the electrical conductivity, we applied the Landauer–Buttiker formalism [43], which determines the amount of current flowing through a given structure as a function of the transparency $T(E,k)$. This function determines the "permeability" of a given structure for electrons (this function is often called the electron transmission function or the transmission function of the conducting channel). Note that the function $T$ for 2D structures is a function of two variables $(E,k)$ and depends on both the electron energy $E$ and the wave number $k$ that determines the electron quasimomentum $p = \hbar k$. To calculate the transmission function, the non-stationary Schrödinger equation was solved using the Keldysh nonequilibrium Green function technique. The Lippmann–Schwinger equation was also used. It allows one to calculate the wave function for a perturbed system in terms of the wave function of the unperturbed system and the Green's operator corresponding to this system. Thus, the electrical conductivity of the material was calculated by the formula:

$$G = \frac{I}{V} = \frac{e^2}{h}\int_{-\infty}^{\infty} T(E)F_T(E-\mu)dE, \quad (2)$$

where $F_T$ and $T(E)$ were defined by the expressions:

$$F_T = \frac{1}{4k_BT}sech^2\left(\frac{E}{2k_BT}\right), \quad (3)$$

$$T(E) = \frac{1}{N}\sum_{k=1}^{N} Tr\left[\Gamma_s(E)G_C^A(E)G_D(E)G_C^R(E)\right], \quad (4)$$

where $T(E)$ is the $k$-averaged electron transmission function (or conductive channel transfer function); $F_T$ is the thermal broadening function, $G_C^A(E), G_C^R(E)$ are the advanced and retarded Green matrices describing contact with electrodes; $\Gamma_s(E), \Gamma_D(E)$ are the broadening matrices for the source and drain [43]. All calculations were performed using the complete basis (s,p) with charge self-consistency. Since supercells contain more than one hundred and even more than two hundred atoms, a unique technique for accelerating such calculations was used to calculate the transmission function [44]. This technique is implemented in the Mizar software package version 1.0 [45]. Using this technique we obtained not only the integral function $T(E)$, which is averaging over all wave numbers, but also a 2D map of the transmission function $T(E,k)$.

## 3. Results and Discussion

We studied two types of SWCNT films: monolayer and bilayer. As indicated above, nanotubes of the achiral type (m, m) for m = 4, 5, 6 and 7 were selected for the study. Monolayer films were a layer of SWCNTs with a distance of ~3.4 Å between nanotubes, which corresponds to the distance between nanotubes in bundles formed during the synthesis of nanotubes. The same distance was observed in bilayer nanotubes, where nanotubes of adjacent layers are mutually perpendicular. Fragments of thin mono- and bilayer films are shown in Figure 1a. The SWCNTs are shown in gray. It should be noted here that the translational step of the periodic cell of SWCNTs must completely coincide with the translational step of the substrate to construct the supercell of the 2D model "SWCNT film + substrate". It is also necessary to ensure that the distance between adjacent SWCNTs coincides with the translation step of the substrate in the direction perpendicular to the nanotube axis. For monolayer films formed by SWCNTs (4,4) and (7,7), this condition for constructing a supercell of 2D model is provided by using a topological model of silicon dioxide—the structure with a space group $P4_2/mnm$, which is characterized by an energy gap $E_{gap}$ equal to 5.50 eV. The surface topology was selected in accordance with the known experimental data on widely used substrates for SWCNTs—

the topology of (100). The thickness of the substrate layer (3 unit cells along the Z axis) was 7.2 Å. The silicon dioxide film retains its dielectric properties at this subnanometer thickness. On the one hand, such a thin silicon dioxide substrate is dielectric-like 3D samples, and on the other hand, it allows the use of high-precision quantum methods in in silico studies. We calculated the energy parameters of the substrate film: the energy gap $E_{gap}$ = 2.30 eV, the Fermi energy $E_F = -6.29$ eV. Another topological model of silicon dioxide was applicable for monolayer films made of SWCNTs (5,5) and (6,6): a structure with the space group $P3_121$ with the (110) surface. The thickness of the substrate film was 7.4 Å. Energy characteristics of this substrate also correspond to dielectric properties: $E_{gap}$ = 3.87 eV, $E_F = -6.29$ eV. Figure 1a shows a fragment of the 2D model "monolayer SWCNT film + substrate" using the example of a film made of SWCNTs (5,5). A model of a fragment of a bilayer film made of SWCNTs (5,5) on a substrate is also presented here. As in the case of a monolayer film, the bilayer film is located on a substrate of the space group $P3_121$ with the (110) surface of the same thickness. The energetically favorable supercell of the 2D model "SWCNT film + substrate" with an intertube distance of 3.4 Å for both layers was constructed only for an SWCNT (5,5) out of all SWCNTs under consideration. In other cases, the step of translation of the substrate and nanotubes did not make it possible to obtain a stable two-layer film on the substrate.

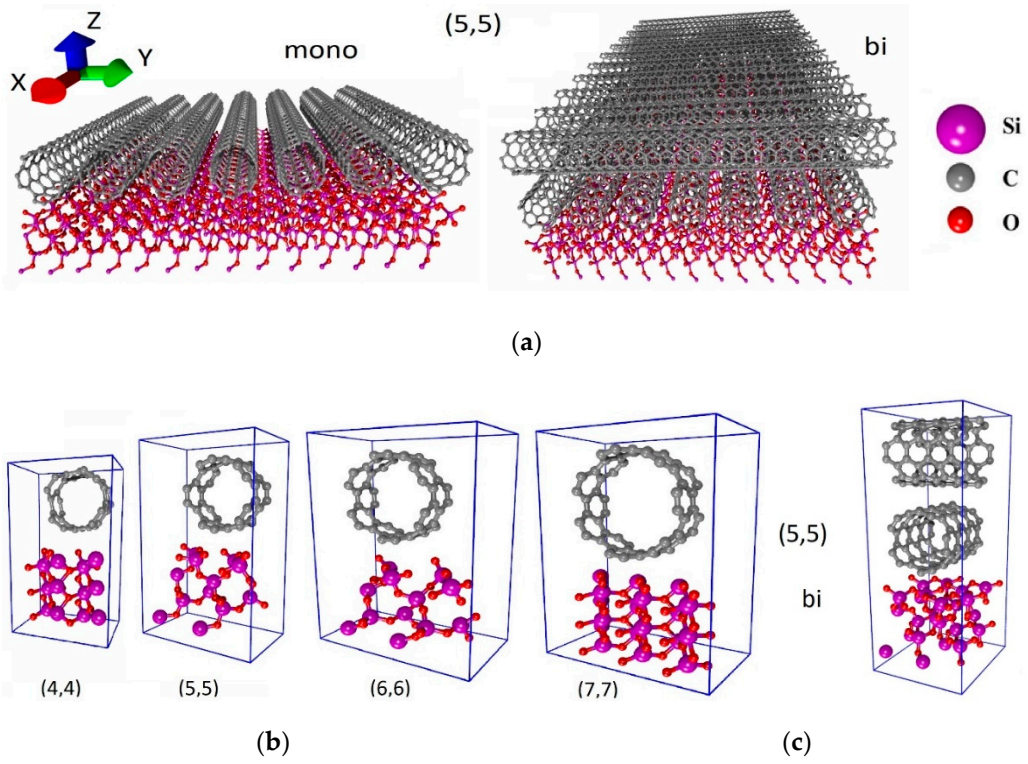


**Figure 1.** Atomistic models of mono- and bilayer films: (**a**) fragments of mono- and bilayer films based on SWCNTs (5,5); (**b**) super-cells of monolayer films; (**c**) super-cell of bilayer film.

Supercells of mono- and bilayer films are shown in Figure 1b,c, respectively. Metric and energy parameters are given for all film models in Table 1. This table presents the translation vectors $L_x$, $L_y$, as well as the number of substrate atoms $N_{at}$ ($SiO_2$) and the total number of the supercell atoms $N_{at}$, the charge transferred to a nanotube $Q_{tube}$, and the Fermi energy. The charge was calculated according to Mulliken. The nanotube-to-substrate distance was ~2.9–3.1 Å for all models. All models were tested at a temperature of 300 K. Table 1 does not provide data on the energy gap, since the carbon films exhibit a metallic type of conductivity in all cases. It can be seen from the table data, the nanotubes "take" the charge from the substrate in all cases. The magnitude of this charge is small, but it introduces certain corrections in the regularities of the electronic properties of films based

on SWCNTs. Especially it is worth paying attention to the bilayer film. As can be seen from the table data, the maximum charge transfer from the substrate was to the bilayer film, which is expected. In this case, the maximum charge transfer ($-0.0213e$) was to the first layer of nanotubes in direct contact with the substrate. The second layer of nanotubes received a much smaller charge and the excess charge was only $-0.0016e$.

**Table 1.** Metric and energy parameters of mono- / bilayer films.

| Parameters | $L_x$, $A$ | $L_y$, $A$ | $Q_{tube}$, $\lvert e \rvert$ | $E_F$, $eV$ | $N_{at}$ | $N_{at}(SiO_2)$ |
|---|---|---|---|---|---|---|
| **Monolayer Film** | | | | | | |
| (4,4) | 8.82 | 4.92 | −0.0021 | −4.28 | 68 | 36 |
| (5,5) | 10.18 | 4.92 | −0.0034 | −3.86 | 76 | 36 |
| (6,6) | 11.54 | 4.92 | −0.0023 | −4.09 | 84 | 36 |
| (7,7) | 12.9 | 4.92 | −0.0079 | −4.37 | 110 | 54 |
| **Bilayer Film** | | | | | | |
| (5,5) | 10.18 | 10.18 | −0.0229 | −3.98 | 232 | 72 |

The densities of electronic states (DOS) are shown in Figure 2 for monolayer films. The DOS plots of the "film + substrate" system and partial DOS for carbon, silicon and oxygen are shown in all cases. Figure 2a shows films with SWCNTs (4,4) and (7,7) located on identical $P4_2/mnm$ substrates with the (100) surface. The DOS plots of oxygen and silicon show a large energy gap, the DOS of oxygen is characterized by a high intensity peak at the top of the valence band. The contribution of carbon becomes noticeable in the conduction band (in the range from −3 to −2.5 eV) and, most importantly, it is carbon that provides non-zero DOS at the Fermi level. Similarly, the DOS plots in Figure 2b are presented for another type of substrate $P3_121$ with the surface (110), on which the films of SWCNTs (5,5) and (6,6) are located. The oxygen intensity peak at the top of the valence band is noticeably lower in this case and its intensity is four times lower than that of the other type of substrate. It is interesting to note that not only the substrate makes a significant contribution to the DOS profile, but the electronic structure of the nanotube also affects the electronic structure of the substrate. This can be clearly seen in Figure 2b, comparing the DOS of oxygen and silicon. The substrate for films with SWCNTs (5,5) and (6,6) is the same, but in the first case, the DOS plots of oxygen and silicon peak at an energy level of −1.7 eV, and in the second case, this peak is absent. The conduction band near the Fermi level of the system "film of SWCNTs (6,6) + substrate" is completely formed by carbon, that is, by nanotubes (the blue and green curves in Figure 2b completely merge above the Fermi level). It can be concluded that the substrate plays an important role in the formation of DOS, and the surface topology determines the degree and nature of the mutual influence of the nanotube and the substrate.

The DOS profile of the "bilayer film + substrate" system is shown in Figure 3a. As expected, the profile in this case almost completely coincides with Figure 2b for a monolayer film, only the intensity of the peaks and DOS values near the Fermi level increased. Analyzing the data in Table 1 and Figures 2 and 3, it can be seen that the substrate also affects the position of the Fermi level. We found that SWCNT films without a substrate are characterized by a Fermi level of $-4.5 \pm 0.4$ eV. However, the influence of the substrate noticeably shifts the Fermi level. In this case, the $P4_2/mnm$ type substrate shifts slightly upward to ~4.3 eV, while the other $P3_121$ substrate already has a much more noticeable effect, shifting the Fermi level to ~4.0 eV, both for mono- and bilayer films. However, the presence of a substrate noticeably shifts the Fermi level. Moreover, if a $P4_2/mnm$ type substrate shifts the Fermi level up to ~4.3 eV, while another $P3_121$ substrate already has a much more noticeable effect, shifting the Fermi level to ~4.0 eV, both for mono- and bilayer films. This is a very important fact, since, on the one hand, the substrate does not reduce the conductivity of the film, and, on the other hand, it decreases the work function of electrons, shifting the Fermi level in the direction of zero electron-volts. This fact is very important for the application of SWCNTs in emission electronics.

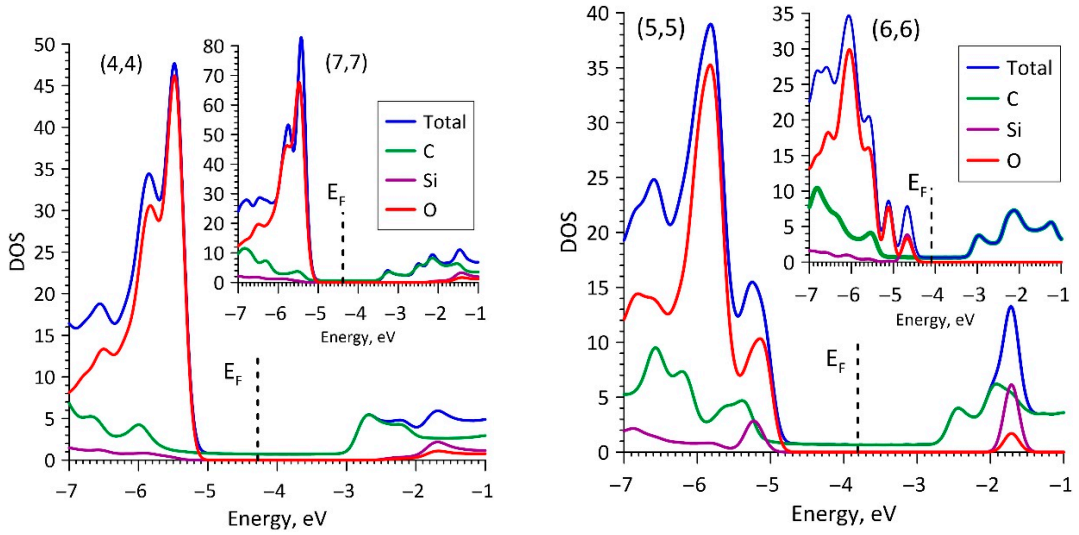


(**a**) (**b**)

**Figure 2.** DOS of monolayer films: (**a**) on the $P4_2/mnm$ substrate with the (100) surface; (**b**) on the $P3_121$ substrate with the surface (110).

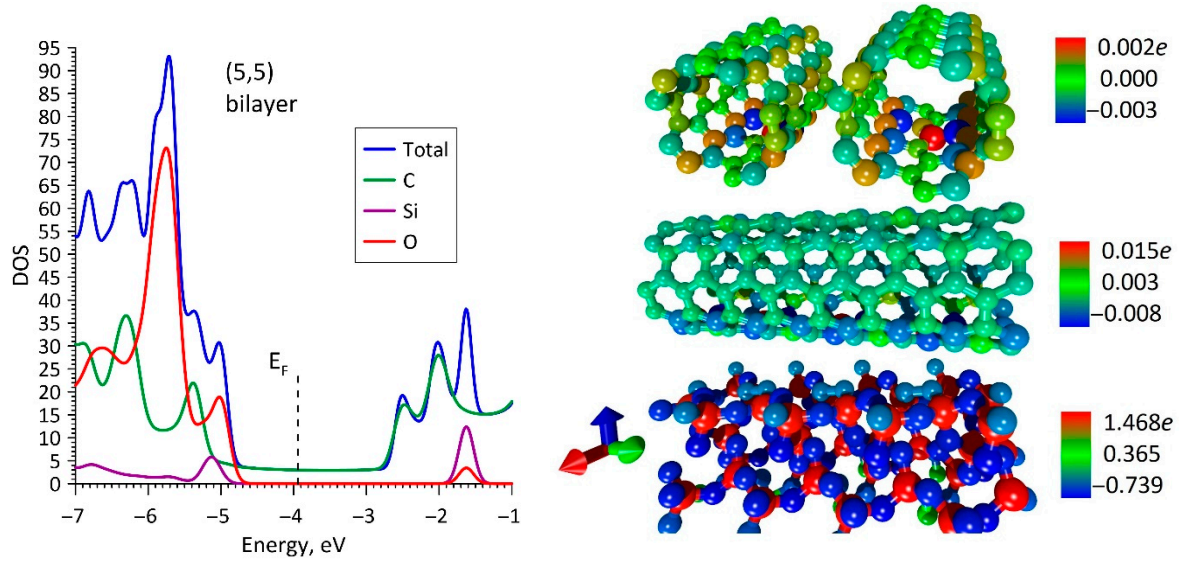


(**a**) (**b**)

**Figure 3.** Electronic characteristics of a bilayer film on a $P3_121$ substrate: (**a**) DOS; (**b**) charge distribution over atoms.

The data in Table 1 demonstrate that there is a charge transfer from the substrate to SWCNTs in all cases. This is especially noticeable in the example of a bilayer film when the double layer of the SWCNT film took almost seven times more charge from the substrate layer. Figure 3b shows the distributions of the electron charge density over the nanotube atoms of both layers and over the atoms of the substrate layer. For the convenience of visualizing charges, this figure shows a fragment of the "bilayer film + substrate" system, which includes two supercells in the Y direction. An analysis of the charge map shows that silicon atoms give a charge to the oxygen atoms of the substrate (almost one electron each), which in turn give a small charge to the atoms of the nanotubes in contact with the surface. All atoms of nanotubes near the substrate carry a negative charge and, according to the results of calculations, the electron charge flows through the lower layer of the nanotubes to the upper one. This may be due to the $\pi$-electrons of nanotubes, which behave quite actively in nanotubes of subnanometer diameter. As is known, thin SWCNTs exhibit the

phenomenon of rehybridization of electron σ- and π-clouds, which leads to an increase in the chemical activity of atoms in such nanotubes. As a consequence, the ionization of the nanotubes leads to noticeable changes in the electronic structure. As shown above, the Fermi level of the "SWCNT film + substrate" system shifts to the right along the energy axis towards zero eV, which leads to a decrease in the electron work function.

The next important stage of our study was to reveal the regularities of the influence of the substrate on the electrical conductivity of the films. The first step in this direction was the calculation of the electron transmission function $T(E,k)$, which depends on the energy and wave number of the first Brillouin zone. This characteristic determines the value of electrical conductivity (see Section 2). Figure 4 shows 2D maps of $T(E,k)$ with a color scale representing the magnitude of the transmission function for different values of energy at different values of the wave number $k$. The values of the transmission function are given in quantum of conductance $e^2/h$, the values of $k$ are given in units of 1/Å. The wavenumber is taken in the direction perpendicular to the direction of current transfer. The electrical conductivity of monolayer films was investigated only along the nanotube axis, that is, along the X-axis. Thus, the wave number on the transmission function maps is represented by the y-component. As is known from the Landauer–Buttiker theory of quantum transport, the x-component of the wave number is taken into account by electrodes that are semi-infinite in the −X and + X directions. Figure 4 also shows the integral transmission functions. 2D maps for the transmission function help to understand the nature of the change in the integral function T(E). For example, in the case of a film of nanotubes (5,5), it can be seen that a wide dip with two minima up to 1 and up to 1.3 eV and with one peak is observed near the Fermi level in the energy range −3.9–−3.83 eV. Such a profile can be explained only by analyzing the color profile of the transmission function map. The minima are formed by deep ravines (blue color) for the intervals $k \in (0; 0.1)$ and (0.2; 0.3). The sharp peak at the energy of −3.87 eV is due to the presence of a ridge (yellow color) with a height of 1.8–2 on the transmission function map for the interval $k$ (0; 0.13). In all other cases, the transmission function maps have a similar form characterized by the presence of two ravines directly at the Fermi level, which leads to a sharp decrease in $T(E)$ near this level. The depth and width of the dip of function $T(E)$ for these films depend on the width of the ravine on the map $T(E, k)$. The $T(E)$ profile of a film of SWCNTs (6,6) has the deepest minimum (up to 0.1) directly at the Fermi level. Indeed, the map data show that the Fermi level passes strictly in the middle of two ravines, which results in a decrease in the integral transmission function. For films of SWCNTs (4,4) and (7,7), this is not observed. The Fermi level passes along the edge of the ravine; therefore, $T(E)$ at this level has a value of 0.9 and 1.1, respectively.

Integral transmission functions and 2D maps of transmission functions were also calculated for the bilayer film. In contrast to monolayer films, bilayer film has electrical conductivity in both X and Y directions; therefore, the transmission functions were calculated for two directions. The calculation results are shown in Figure 5. The presence of two layers of nanotubes leads to increased values of the transmission function for a number of intervals of wave number k. In the case of current transfer in the X direction (the electrical conductivity is provided to the lower layer of the nanotubes), the *T(E, k)* map shows that a ridge of integral function values 2.8–3 (bright yellow color) passes through the entire surface. This ridge is crossed by the Fermi level, which crosses mainly the green field of the map. This led to the fact that the integral function is characterized by a value of 2.1 for $E = E_F$ and to the right of this value. An increased conductivity value can be predicted for this type of film. The conductivity in the Y direction is provided by the top layer of the nanotubes. Here, a completely different character of the surface *T(E, k)* is observed. This difference is explained by different charges on different layers of the film. The lower layer of the film has a higher charge (see Figure 3b), therefore, as expected, the electron transmission function will have higher values in the entire range.

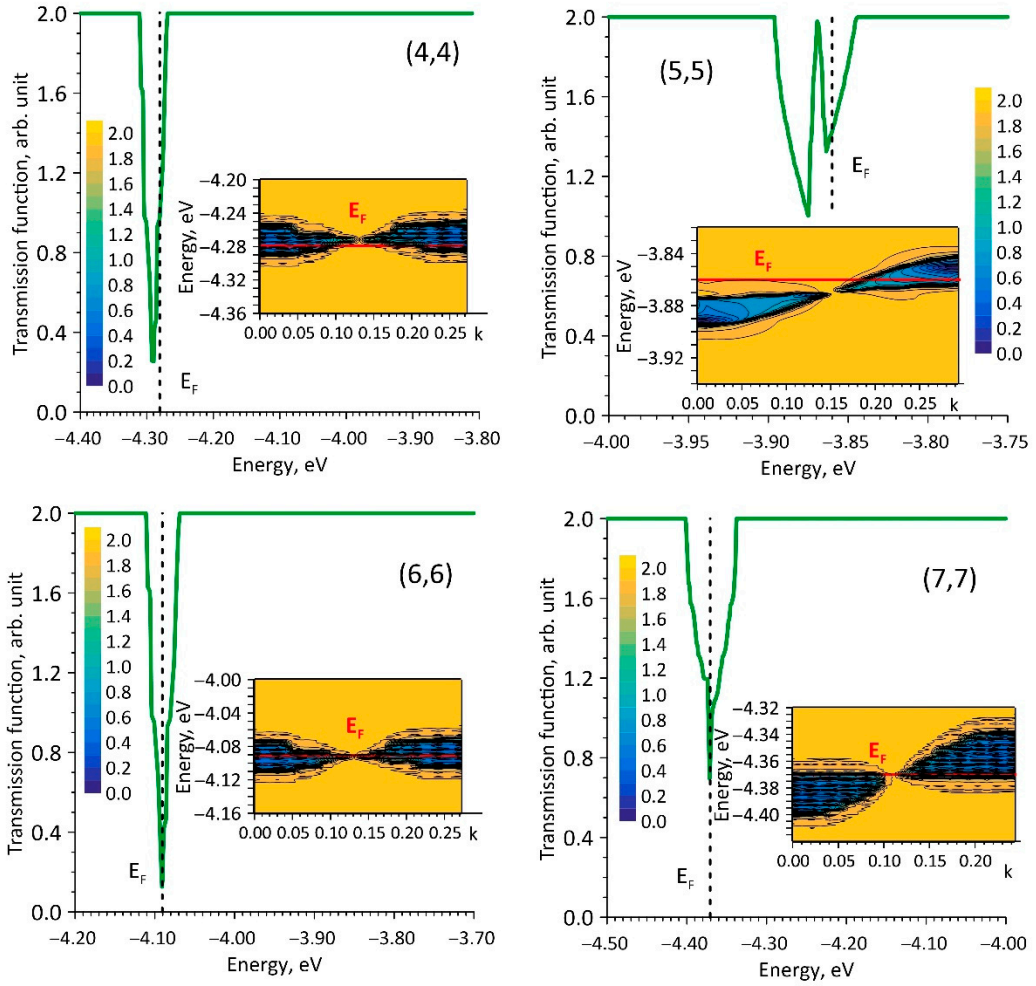


**Figure 4.** Integral transmission functions and 2D maps of transmission functions of monolayer films.

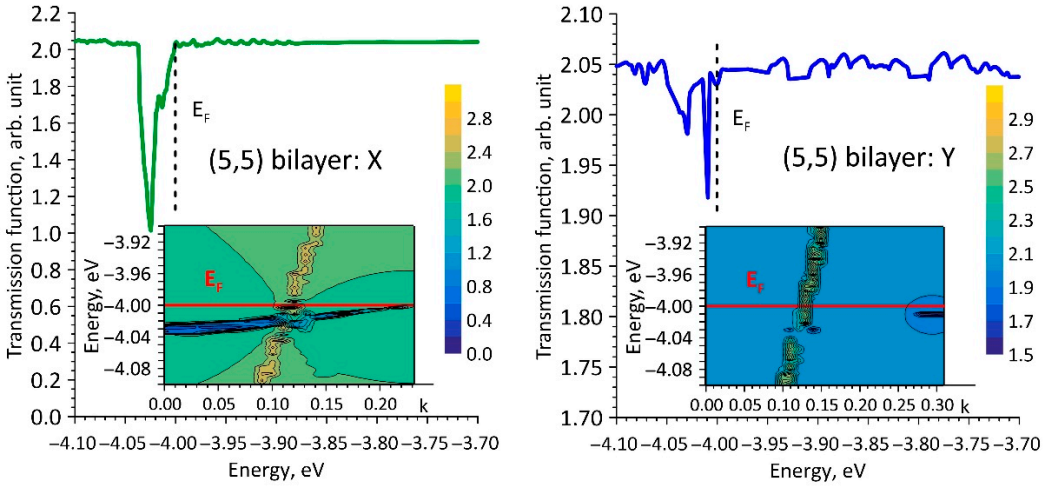


**Figure 5.** Integral transmission functions and 2D maps of transmission functions of bilayer film.

The final stage in the study of the conductivity of films on a substrate was the calculation of the electrical conductivity and resistance, as well as the resistivity. Table 2 presents these electrophysical parameters. This table also shows similar characteristics for mono/bilayer films without substrate. As is known, the minimum resistance for an individual SWCNT is 6.4 kΩ (for nanotubes with two conduction channels at the Fermi level). However, when SWCNTs are combined into tightly packed mono-/bilayer films,

the film resistance differs markedly from 6.4 kΩ. This is explained by the overlapping of π-electron clouds of neighboring nanotubes. As can be seen from the data in Table 2, all single-walled nanotube films are characterized by a resistance that is much greater than ~7–8 kOhm as compared to 6.4 kOhm. The minimum resistance value for a monolayer film is 6.867 kΩ. This is due to natural reasons for the redistribution of the electronic charge between the film and the substrate. However, the picture changes markedly for a film of two layers of nanotubes. In the absence of a substrate, the resistance of each of the film layers was close to a value of ideal SWCNT and amounted to ~6.43 kΩ, while in the presence of a substrate it practically did not change. The resistance of the upper layer of the bilayer film tubes was 6.438 kΩ, which practically does not differ from the resistance values for the film without a substrate.

**Table 2.** Electrophysical parameters of films on a substrate.

| Parameters | (4,4) | (5,5) | (6,6) | (7,7) | (5,5)-X Bilayer | (5,5)-Y Bilayer |
|---|---|---|---|---|---|---|
| **Films on a Substrate** | | | | | | |
| G, μS | 123.824 | 132.686 | 144.638 | 123.528 | 148.005 | 155.312 |
| R, kOhm | 8.076 | 7.537 | 6.913 | 8.095 | 6.800 | 6.438 |
| **Films without Backing** | | | | | | |
| G, μS | 121.045 | 145.619 | 134.027 | 144.914 | 155.312 | 155.312 |
| R, kOhm | 8.261 | 6.867 | 7.461 | 6.900 | 6.438 | 6.431 |

## 4. Conclusions

An in silico study of the influence of the electronic structure of a silicon dioxide substrate on the electrical conductivity of mono- and bilayer films made of armchair SWCNTs was carried out. The thin film of silicon dioxide with a thickness of 7.2 Å was taken as a substrate. This choice is due to the limitation of the atomic composition of the supercell for quantum-mechanical calculations of the electronic structure, as well as quantum calculations of electron transport using the apparatus of Green's functions. However, the selected thin film retains the inherent dielectric properties of 3D-$SiO_2$. Among the considered armchair SWCNTs with a diameter of 0.5–1 nm, including SWCNTs (4,4), (5,5), (6,6), and (7,7), supercells of monolayer films on a substrate were constructed for all nanotubes, but for a bilayer film, it was possible to construct only one supercell for an SWCNT film (5,5).

It was found that the dielectric substrate affects the conductivity of a monolayer film of carbon nanotubes, increasing the resistance by 10–17% in some cases, or, conversely, decreasing it by 2–7%. As for the only model of a bilayer film, then we can say that the substrate has practically no effect on the electrical conductivity and resistance of the film in both directions differs slightly from the data for a film without a substrate. In this case, the resistance values approach the value of ~6.4 kOhm, which is the minimum resistance for an individual SWCNT.

It was noted that the crystalline phase of the substrate does not play a decisive role, but the decisive role is still played by the number of nanotube layers in the film.

**Author Contributions:** Conceptualization, O.E.G.; methodology, O.E.G.; funding acquisition, M.M.S., O.E.G.; investigation, O.E.G., A.A.P. and M.M.S.; writing—original draft preparation, A.A.P.; writing—review and editing, M.M.S. and O.E.G.; supervision, O.E.G. All authors have read and agreed to the published version of the manuscript.

**Funding:** The research of electrical conductivity of mono- and bilayer SWCNT films was funded by the Ministry of Science and Higher Education of the Russian Federation in the framework of the government task (project No. FSRR-2020-0004), the research of electronic properties of mono- and bilayer SWCNT films was funded by the Council on grants of the President of the Russian Federation (project No. MK-2289.2021.1.2).

**Conflicts of Interest:** The authors declare no conflict of interest.

## References


1. Jiang, S.; Hou, P.X.; Chen, M.L.; Wang, B.W.; Sun, D.M.; Tang, D.M.; Jin, Q.; Guo, Q.X.; Zhang, D.D.; Du, J.H.; et al. Ultrahigh-performance transparent conductive films of carbon-welded isolated single-wall carbon nanotubes. *Sci. Adv.* **2018**, *4*, eaap9264. [CrossRef] [PubMed]
2. Devaraju, S.; Lee, T.; Mohanty, A.K.; Hong, Y.K.; Yoon, K.H.; Lee, Y.S.; Han, J.H.; Paik, H.J. Fabrication of durable and flexible single-walled carbon nanotube transparent conductive films. *RSC Adv.* **2017**, *7*, 19267–19272. [CrossRef]
3. Siwal, S.S.; Saini, A.K.; Rarotra, S.; Zhang, Q.; Thakur, V. Recent advancements in transparent carbon nanotube films: Chemistry and imminent challenges. *J. Nanostruct. Chem.* **2021**, *11*, 93–130. [CrossRef]
4. Qu, S.; Dai, Y.; Zhang, D.; Li, Q.; Chou, T.; Weibang, L. Carbon nanotube film based multifunctional composite materials: An overview. *Funct. Compos. Struct.* **2020**, *2*, 022002. [CrossRef]
5. Zhang, Q.; Zhou, W.; Xia, X.; Li, K.; Zhang, N.; Wang, Y.; Xiao, Z.; Fan, Q.; Kauppinen, E.; Xie, S. Transparent and Freestanding Single-Walled Carbon Nanotube Films Synthesized Directly and Continuously via a Blown Aerosol Technique. *Adv. Mater.* **2020**, *32*, 2004277. [CrossRef] [PubMed]
6. Mirri, F.; Ma, A.W.; Hsu, T.T.; Behabtu, N.; Eichmann, S.L.; Young, C.C.; Tsentalovich, D.E.; Pasquali, M. High-Performance Carbon Nanotube Transparent Conductive Films by Scalable Dip Coating. *ACS Nano* **2012**, *6*, 9737–9744. [CrossRef]
7. Shimoni, A.; Azoubel, S.; Magdassi, S. Inkjet printing of flexible high-performance carbon nanotube transparent conductive films by "coffee ring effect". *Nanoscale* **2014**, *6*, 11084–11089. [CrossRef] [PubMed]
8. Yu, W.; Zhou, H.; Li, B.Q.; Ding, S. 3D Printing of Carbon Nanotubes-Based Microsupercapacitors. *ACS Appl. Mater. Interfaces* **2017**, *9*, 4597–4604. [CrossRef]
9. Sweeney, C.B.; Lackey, B.A.; Pospisil, M.J.; Achee, T.C.; Hicks, V.K.; Moran, A.G.; Teipel, B.R.; Saed, M.A.; Green, M.J. Welding of 3D-printed carbon nanotube–polymer composites by locally induced microwave heating. *Sci. Adv.* **2017**, *3*, e1700262. [CrossRef] [PubMed]
10. Mustonen, K.; Nasibulin, A.G.; Pudas, M.; Kauppinen, M.; Jiang, H.; Grigoras, K.; Raula, J.; Kauppinen, E.I. Reinforcing randomly oriented transparent freestanding single-walled carbon nanotube films. *Carbon* **2013**, *62*, 513–516. [CrossRef]
11. Bu, Q.; Zhan, Y.; He, F.; Lavorgna, M.; Xia, H. Stretchable conductive films based on carbon nanomaterials prepared by spray coating. *J. Appl. Polym. Sci.* **2016**, *133*, 43243. [CrossRef]
12. De Volder, M.F.; Tawfick, S.H.; Baughman, R.H.; Hart, A.J. Carbon nanotubes: Present and future commercial applications. *Science* **2013**, *339*, 535–539. [CrossRef]
13. Zhou, Y.; Azumi, R. Carbon nanotube based transparent conductive films: Progress, challenges, and perspectives. *Sci. Technol. Adv. Mater.* **2016**, *17*, 493–516. [CrossRef]
14. Huang, J.; Zhu, Y.; Jiang, W.; Yin, J.; Tang, Q.; Yang, X. Parallel carbon nanotube stripes in polymer thin film with remarkable conductive anisotropy. *ACS Appl. Mater. Interfaces* **2014**, *6*, 1754–1758. [CrossRef]
15. Dong, C.; Hao, J. Ordered porous films of single-walled carbon nanotubes using an ionic exchange reaction. *Colloids Surf. A Physicochem. Eng. Asp.* **2019**, *566*, 207–217. [CrossRef]
16. Sajed, F.; Rutherglen, C. All-printed and transparent single walled carbon nanotube thin film transistor devices. *Appl. Phys. Lett.* **2013**, *103*, 143303. [CrossRef]
17. Bandodkar, A.J.; Jeerapan, I.; You, J.M.; Nuñez-Flores, R.; Wang, J. Highly Stretchable Fully-Printed CNT-Based Electrochemical Sensors and Biofuel Cells: Combining Intrinsic and Design-Induced Stretchability. *Nano Lett.* **2016**, *16*, 721–727. [CrossRef] [PubMed]
18. Wang, C.; Takei, K.; Takahashi, T.; Javey, A. Carbon nanotube electronics—Moving forward. *Chem. Soc. Rev.* **2013**, *42*, 2592–2609. [CrossRef]
19. Cai, L.; Wang, C. Carbon Nanotube Flexible and Stretchable Electronics. *Nanoscale Res. Lett.* **2015**, *10*, 320. [CrossRef] [PubMed]
20. Cai, L.; Song, L.; Luan, P.; Zhang, Q.; Zhang, N.; Gao, Q.; Zhao, D.; Zhang, X.; Tu, M.; Yang, F.; et al. Super-stretchable, transparent carbon nanotube-based capacitive strain sensors for human motion detection. *Sci. Rep.* **2013**, *3*, 3048. [CrossRef]
21. Dinh, T.; Phan, H.P.; Nguyen Tuan, K.; Qamar, A.; Md Foisal, A.; Viet, T.N.; Tran, C.D.; Zhu, Y.; Nguyen, N.T.; Dao, D. Environment-friendly carbon nanotube based flexible electronics for noninvasive and wearable healthcare. *J. Mater. Chem. C* **2016**, *4*, 10061–10068. [CrossRef]
22. Lv, X.; Deng, J.; Wang, B.; Zhong, J.; Sham, T.K.; Sun, X.; Sun, X. $\gamma$-$Fe_2O_3$@CNTs Anode Materials for Lithium Ion Batteries Investigated by Electron Energy Loss Spectroscopy. *Chem. Mater.* **2017**, *29*, 3499–3506. [CrossRef]
23. Franklin, A.D.; Chen, Z.H. Length scaling of carbon nanotube transistors. *Nat. Nanotech.* **2010**, *5*, 858–862. [CrossRef]
24. Franklin, A.D.; Luisier, M.; Han, S.J.; Tulevski, G.; Breslin, C.M.; Gignac, L.; Lundstrom, M.S.; Haensch, W. Sub-10 nm carbon nanotube transistor. *Nano. Lett.* **2012**, *12*, 758–762. [CrossRef] [PubMed]
25. Qiu, C.; Zhang, Z.; Xiao, M.; Yang, Y.; Zhong, D.; Peng, L. Scaling carbon nanotube complementary transistors to 5-nm gate lengths. *Science* **2017**, *355*, 271–276. [CrossRef]
26. Xu, L.; Qiu, C.; Peng, L.-M.; Zhang, Z. Suppression of leakage current in carbon nanotube field-effect transistors. *Nano Res.* **2021**, *14*, 976–981. [CrossRef]
27. Franklin, A.D. Te road to carbon nanotube transistors. *Nature* **2013**, *498*, 443–444. [CrossRef] [PubMed]

28. Zhong, D.; Zhang, Z.; Ding, L.; Han, J.; Xiao, M.; Si, J.; Xu, L.; Qiu, C.; Peng, L. Gigahertz integrated circuits based on carbon nanotube films. *Nat. Electron.* **2018**, *1*, 40–45. [CrossRef]
29. Xie, Y.; Zhang, Z.; Zhong, D.; Peng, L. Speeding up carbon nanotube integrated circuits through three-dimensional architecture. *Nano Res.* **2019**, *12*, 1810–1816. [CrossRef]
30. Liu, L.; Ding, L.; Zhong, D.; Han, J.; Wang, S.; Meng, Q.; Qiu, C.; Zhang, X.; Peng, L.M.; Zhang, Z. Carbon Nanotube Complementary Gigahertz Integrated Circuits and Their Applications on Wireless Sensor Interface Systems. *ACS Nano* **2019**, *13*, 2526–2535. [CrossRef]
31. Liu, Z.; Zhao, J.; Xu, W.; Qian, L.; Nie, S.; Cui, Z. Effect of surface wettability properties on the electrical properties of printed carbon nanotube thin-film transistors on $SiO_2$/Si substrates. *ACS Appl. Mater. Interfaces* **2014**, *6*, 9997–10004. [CrossRef]
32. Xiang, L.; Zhang, H.; Dong, G.; Zhong, D.; Han, J.; Liang, X.; Zhang, Z.; Peng, L.-M.; Hu, Y. Low-Power Carbon Nanotube-Based Integrated Circuits that Can be Transferred to Biological Surface. *Nat. Electron.* **2018**, *1*, 237–245. [CrossRef]
33. Li, X.; Zhu, Y.; Cai, W.; Borysiak, M.; Han, B.; Chen, D.; Piner, R.D.; Colombo, L.; Ruoff, R.S. Transfer of Large-Area Graphene Films for High-Performance Transparent Conductive Electrodes. *Nano Lett.* **2009**, *9*, 4359–4363. [CrossRef] [PubMed]
34. Liu, S.; Guo, X. Carbon nanomaterials field-effect-transistor-based biosensors. *NPG Asia Mater.* **2012**, *4*, e23. [CrossRef]
35. Elstner, M.; Porezag, D.; Jungnickel, G.; Elsner, J.; Haugk, M.; Frauenheim, T.; Suhai, S.; Seifert, G. Self-consistent-charge density-functional tight-binding method for simulations of complex materials properties. *Phys. Rev. B* **1998**, *58*, 7260–7268. [CrossRef]
36. Elstner, M.; Seifert, G. Density functional tight binding. *Phil. Trans. R. Soc. A* **2014**, *372*, 20120483. [CrossRef]
37. Ghorbani-Asl, M.; Bristowe, P.D.; Koziol, K. A computational study of the quantum transport properties of a Cu-CNT composite. *Phys. Chem. Chem. Phys.* **2015**, *17*, 18273–18277. [CrossRef]
38. Naumov, V.S.; Loginova, A.S.; Avdoshin, A.A.; Ignatov, S.; Mayorov, A.V.; Aradi, B.; Frauenheim, T. Structural, electronic, and thermodynamic properties of $TiO_2$/organic clusters: Performance of DFTB method with different parameter sets. *Int. J. Quantum Chem.* **2021**, *121*, e26427. [CrossRef]
39. Slepchenkov, M.M.; Shmygin, D.S.; Zhang, G.; Glukhova, O.E. Controlling anisotropic electrical conductivity in porous graphene-nanotube thin films. *Carbon* **2020**, *165*, 139–149. [CrossRef]
40. Rappe, A.K.; Casewit, C.J.; Colwell, K.S.; Goddard III, W.A.; Skiff, W.M. UFF, a full periodic table force field for molecular mechanics and molecular dynamics simulations. *J. Am. Chem. Soc.* **1992**, *114*, 10024–10035. [CrossRef]
41. DFTB+ Density Functional Based Tight Binding (and More). Available online: https://dftbplus.org/ (accessed on 10 October 2020).
42. Hourahine, B.; Aradi, B.; Blum, V.; Bonafé, F.; Buccheri, A.; Camacho, C.; Cevallos, C.; Deshaye, M.Y.; Dumitrică, T.; Dominguez, A.; et al. DFTB+, a software package for efficient approximate density functional theory based atomistic simulations. *J. Chem. Phys.* **2020**, *152*, 124101. [CrossRef]
43. Datta, S. *Quantum Transport.: Atom. to Transistor*, 2nd ed.; Cambridge University Press: New York, NY, USA, 2005; pp. 217–251.
44. Glukhova, O.E.; Shmygin, D.S. The electrical conductivity of CNT/graphene composites: A new method for accelerating transmission function calculations. *Beilstein. J. Nanotechnol.* **2018**, *9*, 1254–1262. [CrossRef]
45. Software Package Mizar. Available online: Nanokvazar.ru/ (accessed on 8 November 2020).